Volume 52
Number 42
14 November 2023
Pages 15135-15610

Dalton Transactions

An international journal of inorganic chemistry

rsc.li/dalton

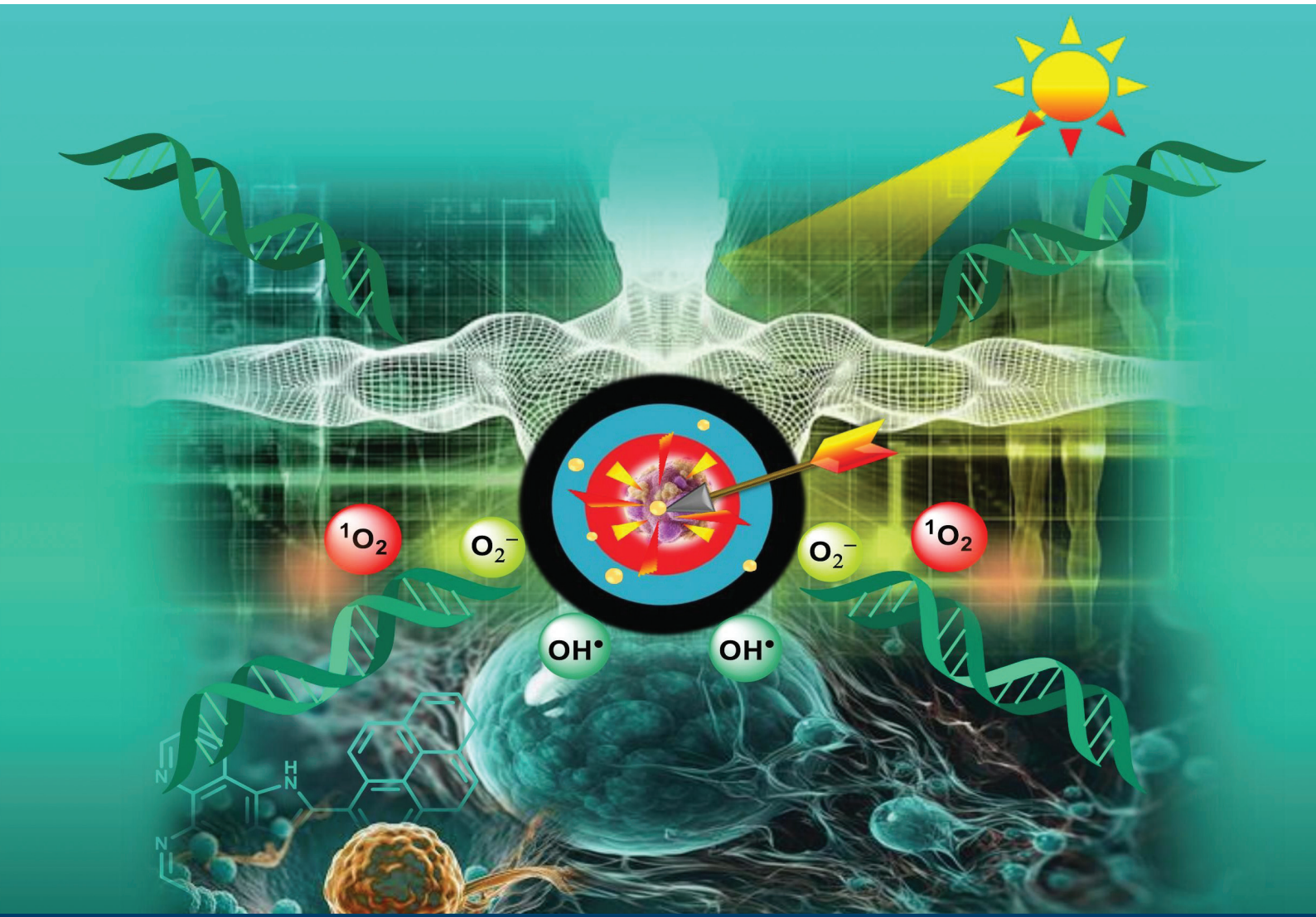

Themed issue: New Talent: Asia Pacific

ISSN 1477-9226

ROYAL SOCIETY OF CHEMISTRY

PAPER

Rishav Das and Priyankar Paira

GSH resistant, luminescent 2-(pyren-1-yl)-1*H*-imidazo[4,5-*f*][1,10]phenanthroline-based Ru(II)/Ir(III)/Re(I) complexes for phototoxicity in triple-negative breast cancer cells

Dalton Transactions

ROYAL SOCIETY OF CHEMISTRY

PAPER

View Article Online
View Journal | View Issue

Cite this: *Dalton Trans.*, 2023, **52**, 15365

GSH resistant, luminescent 2-(pyren-1-yl)-1*H*-imidazo[4,5-*f*][1,10]phenanthroline-based Ru(II)/Ir(III)/Re(I) complexes for phototoxicity in triple-negative breast cancer cells†

Rishav Das and Priyankar Paira *

Selective chemotherapeutic strategies necessitate the emergence of a photosensitive scaffold to abate the nuisance of cancer. In the current context, photo-activated chemotherapy (PACT) has, therefore, appeared to be very effective to vanquish the vehemence of triple-negative breast cancer (TNBC). Metal complexes have been identified to act well against cancer cell microenvironment (high GSH content, low pH, and hypoxia), and thus they have been employed in the treatment of various types of cancer. As TNBC is very challenging to treat owing to its poor prognosis, lack of a specific target, high chance of relapse, and strong metastatic ability, herein we have aspired to design GSH-resistant phototoxic Ru(II)/Ir(III)/Re(I) based pyrene imidazophenathroline complexes to selectively avert the triple-negative breast cancer. The application of complexes, [**RuL**], [**IrL**], and [**ReL**] in the absence and in the presence of GSH against MDA-MB-231TNBC cells, has revealed that they are very active upon irradiation of visible light compared to dark due to the creation of copious singlet oxygen ($^1O_2$) as reactive oxygen species (ROS). Among three synthesized complexes, [**IrL**] has shown outstanding potency (IC_{50} = 3.70 in the absence of GSH and IC_{50} = 3.90 in the presence of GSH). Also, the complex, [**IrL**] is capable of interacting with DNA with the highest binding constant ($K_b = 0.023 \times 10^6$ M^{-1}) along with higher protein binding affinity ($K_{BSA} = 0.0321 \times 10^6$ M^{-1}). Here, it has been unveiled that all the complexes have been entitled to involve DNA covalent interaction through the available sites of both adenine and guanine bases.

Received 31st May 2023,
Accepted 12th July 2023

DOI: 10.1039/d3dt01667f

rsc.li/dalton

1. Introduction

In clinical terminology, triple-negative breast cancer (TNBC) can be characterized as a very obnoxious phenotype of breast cancer, which lacks the expression of estrogen receptor (ER), progesterone receptor (PgR), and human epidermal growth factor receptor 2 (HER2).[1] The American Society of Clinical Oncology (ASCO) has estimated that the cellular expression of ER and PgR in TNBC is ≤1% and the expression of HER2 is in the range of 0 to +1 based on immunohistochemistry (IHC).[2] It has been documented that mutations occurring in BRCA1 and BRCA2 genes can be regarded as one of the prime causes of TNBC (Shiovitz and Korde, 2015).[3] In addition to this, mutations in CDH1, TP53, STK11, and PTEN have been proven to be allied with the occurrence of different kinds of breast cancers (BCs) as well as of TNBCs.[4] Statistical report has unveiled that mostly females are more prone for TNBC in comparison to males due to the stimulation of different sex hormones, and approximately 170 000 are victims of TNBC in 1 million cases of breast cancer annually.[5,6] Several physiological modifications occur in endogenous sex hormones, plunging the premenopausal and postmenopausal women into a higher risk of breast cancer (BC).[7] On the other hand, the basal metabolic index (BMI) can also impart an important reason for causing breast cancer (BC).[8] It has been noticed that women above 50 years old having greater BMI, become a prey of breast cancer (BC) at a higher risk compared to those with lower BMI.[9] The heterogeneity of TNBC with poor prognosis and high rate of metastasis in the brain, bone, lungs, *etc.*, cause high rate of recurrence, and the absence of prominent therapeutic targets (ER−/PgR−/HER2−) has made TNBC very perilous to the living world.[10] Therefore, to abate the aggressive prevalence of TNBC, the development of proper therapeutic routes has become an urgent issue for both researchers and clinicians in recent anticancer research. Among the various treatment modalities (radiotherapy, surgery, hormonal therapy, *etc.*), chemotherapy has been seen as an effective method to treat TNBC, wherein, the treatment strategy may be the impairing of DNA and suppression of overexpressed onco-

Department of Chemistry, School of advanced sciences, Vellore Institute of Technology, Vellore-632014, Tamilnadu, India. E-mail: priyankar.paira@vit.ac.in

† Electronic supplementary information (ESI) available. See DOI: https://doi.org/10.1039/d3dt01667f

genes, targeting some specific organelle in order to cease cancer cell proliferation.[11] Metal complexes have proven to be very proficient anticancer chemotherapeutic agents after the discovery of cisplatin in 1965.[12] Although cisplatin showed promising anticancer activity for the treatment of TNBC, various side effects associated with it, compelled the researchers to develop some other metal complexes with minimal side effects.[13] On the way of ongoing research, ruthenium, iridium, and rhenium based metal complexes came out as pertinent alternatives to overcome the drawbacks of cisplatin due to their astounding photophysical properties and stability under cancer cell microenvironment along with a higher degree of cytoselectivity.[14] However, in order to achieve the utmost selective treatment strategy, photo-activated chemotherapy (PACT) is now being efficaciously employed in oxygen-deficient (hypoxia) conditions.[15] Consequently, in 2017, TLD1433 was developed by the McFarland group as the first Ru(II)-based photosensitizer, applicable for photodynamic therapy (PDT), and has undergone clinical trials.[16] The anticancer ruthenium complexes have been fascinating the interest of researchers for a long period as a result of their capability to be active against cisplatin-resistant tumors and to target specifically metastasized solid tumors.[17] The proficiency of Ru(II)-based PACT agents mostly depends on their photoinduced ligand dissociation ability.[18] S. Bonnet *et al.* synthesized a few bisquinoline chelating ruthenium complexes as PACT agents. Then, they studied their photochemistry and phototoxic behaviour in order to evaluate their applicability in photo-activated chemotherapy (PACT).[19] C. F. Daher *et al.* reported a series of photoactivable strained Ru(II)-polypyridyl complexes and showed that these complexes were highly potent against MDA-MB-231 triple-negative breast cancer cells.[20] In connection with the ruthenium complexes, iridium complexes are also very adept in exhibiting photo-induced chemotherapeutic potential. H. Chao and co-workers prepared some photosensitive phosphorescent Ir(III) complexes, which were capable of causing mitochondrial dysfunction by generating ROS.[21] W. Gao *et al.* synthesized a few lysosome-targeted phosphorescent Ir(III) complexes, which showed profound phototoxicity.[22] P. J. Sadler *et al.* reported a group of photosensitive organoiridium-albumin conjugates, which targeted nuclear DNA and were applicable for photodynamic therapy (PDT).[23] Y. Zhao *et al.* developed some cyclometalated Ir(III) based micelles for GSH-responsive targeted chemotherapy along with photodynamic therapy (PDT).[24] Again, rhenium tricarbonyl complexes, $(CO)_3$Re(I) are well-known to generate singlet oxygen ($^1O_2$) in a lipophilic environment displaying high quantum yield.[25] The selectivity of Re-photosensitizers towards various cancer cells, can be improved by combining the moiety with a variety of biologically significant targeting molecules, which includes folic acid, biotin, and cell-permeable peptides.[26] G. Gasser *et al.* synthesized a few rhenium(I) tricarbonyl complexes, which were very competent to cause DNA photo-cleavage *via* the production of singlet oxygen ($^1O_2$) and very minor extent of superoxide under irradiation of light.[27] E. Meggers *et al.* developed the pyridocarbazole-based Re(I) complexes with a pyridine ancillary ligand. These complexes were able to induce apoptosis upon irradiation of light ($\lambda \geq 505$ nm) producing an ample amount of $^1O_2$, but they were less toxic in the dark.[28] J. J. Wilson and co-workers synthesized phototoxic Re(I) tricarbonyl complexes possessing water-soluble tris(hydroxymethyl)phosphine (THP) ligand and 1,3,7-triaza-5- phosphabicylco[3.3.1]nonane (DAPTA) ligand. This research group showed that upon irradiation of light, these complexes were highly toxic towards human ovarian (A2780), cervical (HeLa), and cisplatin-resistant ovarian (A2780CP70) cancer cell lines but they were incapable of exhibiting toxicity in the absence of light.[29]

Together with the benefits of Ru(II), Ir(III), and Re(I) metals, the construction of ligands is very influential in order to have anticipated biological activities of the metal complexes. For a long time since, pyrene has been recognized as a well-known class of polycyclic aromatic hydrocarbons (PAHs), which are convoyed with their intrinsic anticancer activities.[30] F. F. Becker *et al.* developed some pyrene derivatives and showcased their anticancer activities against B_{16}, BRO, MCF-7, OVCAR3, $P_{388/0}$, PC3, HT-29 cancer cell lines.[31] G. Barone *et al.* reported pyrene-imidazolium derivatives, which were observed to be very apt in displaying excellent DNA binding affinity to G-quadruplex (G4) DNA where G4-DNA comprises of short tracts of guanine-augmented sequences flourished with the capabilities to crease into tetrads in which each guanine moiety is connected to the other by dint of Hoogsten hydrogen bonds.[32] In line with this, our research group has proved the importance of imidazophenanthroline moiety in anticancer activity, several times.[33,34] Therefore, in the present work, we have intended to synthesize a new class of pyrene imidazophenathroline based ruthenium(II), iridium(III), and rhenium(I) organometallic complexes in order to embellish phototoxic proficiency into them. Herein, we have developed three complexes, [**RuL**], [**IrL**] and [**ReL**], which have been designed in order to assimilate the following qualities: they will be (a) photoactive for selective chemotherapy having the capability of $^1O_2$ generation, (b) stable under cancer cell environment (high GSH, low pH, hypoxic), (c) susceptible to bind with plasma protein to be delivered to the target cells, (d) permeable through the plasma membrane, (e) luminescent for cellular tracking, (f) efficient in interaction with DNA through either covalent or non-covalent manner and (g) ultimately will be active to annihilate the cancer cell by preventing the cancer cell proliferation (Fig. 1).

2. Results and discussion

Synthesis and characterization

The synthesis of ligand **L** and its respective [**RuL**] [**IrL**] [**ReL**] complexes is summarized in Scheme 1. To synthesize 2-(pyrene-1-yl)-1*H*-imidazo[4,5-*f*] [1,10] phenanthroline (**L**), 1,10-phenanthroline-5,6-dione (1 equiv.) was treated with pyrene-1-carboxaldehyde (1 equiv.) in the presence of minimum glacial acetic acid as solvent and excess ammonium acetate as the

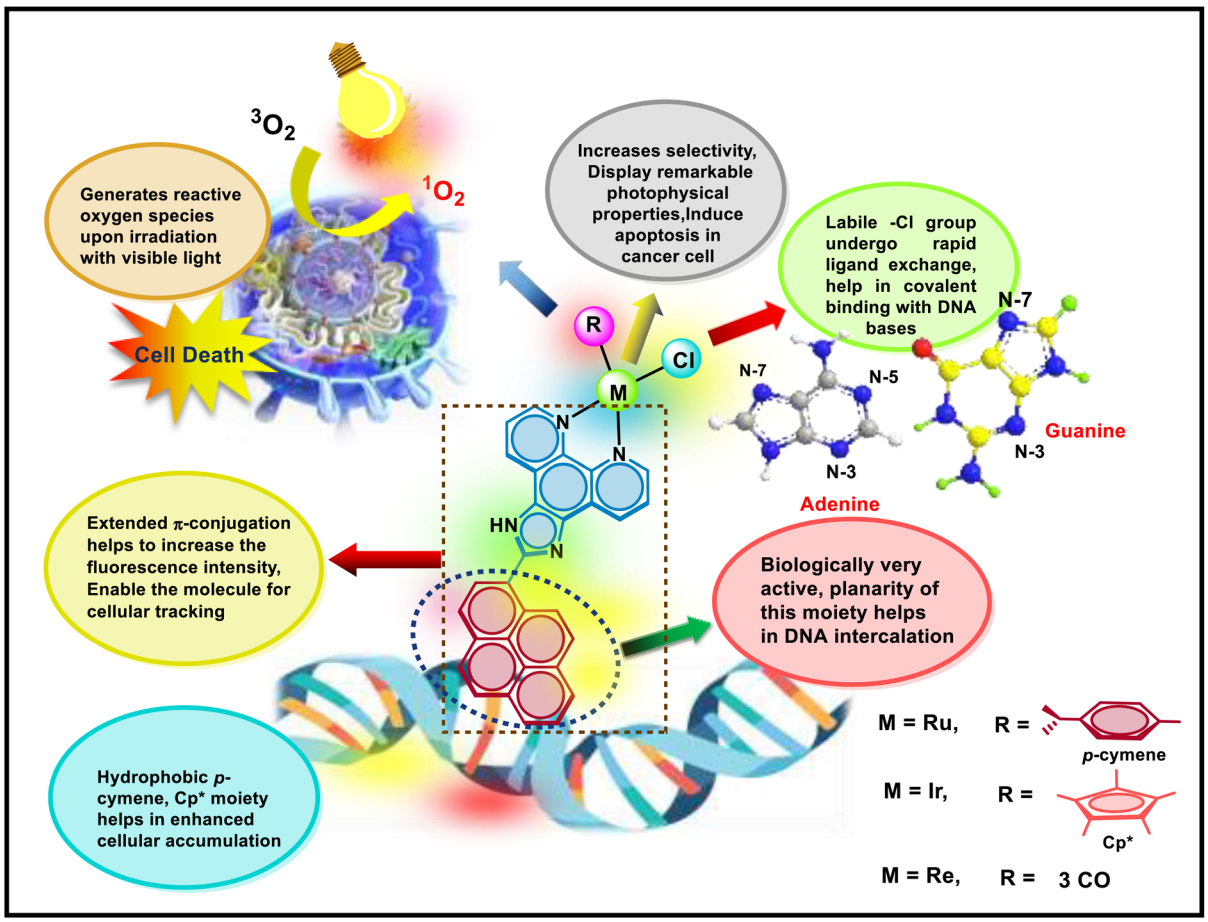

Fig. 1 Design of (Ru, Ir and Re)-based 2-(pyren-1-yl)-1*H*-imidazo[4,5-*f*][1,10]phenanthroline complexes, [**RuL**], [**IrL**] and [**ReL**].

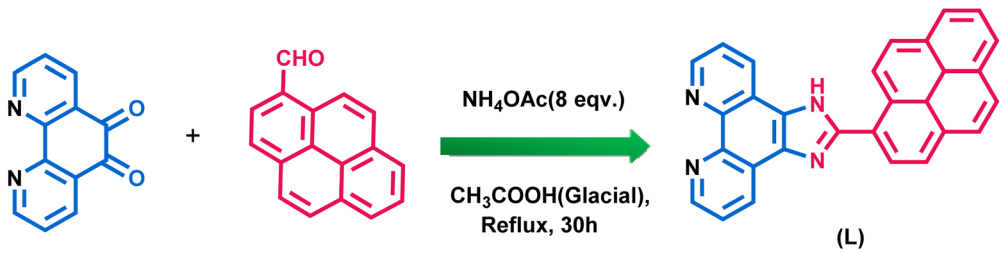

Scheme 1 Synthesis of ligand (**L**).

base. The characterization was performed by ^{1}H and ^{13}C nuclear magnetic resonance (NMR), Fourier transform infrared spectroscopy (FT-IR), and high-resolution mass spectrometry (HRMS). In ^{1}H NMR spectrum of 2-(pyrene-1-yl)-1*H*-imidazo [4,5-*f*] [1,10] phenanthroline, the most downfield proton appeared in δ 9.57 ppm as a doublet. All other aromatic protons are displayed at δ 7.91–9.09 ppm. In the ^{13}C NMR spectrum, all peaks were found at δ 123.90–148.42 ppm. The IR stretching frequency of C–N was observed as 1402.88 cm^{-1}, which supported the formation of the C–N bond. From ESI-MS, *m*/*z* value 443.1277 $[M + Na]^+$ was exactly matched with the calculated value (Scheme 2).

Iridium(III)Cp*[2-(pyrene-1-yl)-1*H*-imidazo[4,5-*f*][1,10]phenanthroline]chloride [**IrL**] was synthesized by adding the Ir precursor, $[(\eta^5\text{-Cp}^*)\text{IrCl}(\mu\text{-Cl})]_2$ (0.5 equiv.) in a methanolic solution of ligand **L** (1 equiv.) under stirring for 2 h in ambient temperature. The structure of this complex was characterized by ^{1}H and ^{13}C NMR, FT-IR, and HRMS. In the ^{1}H NMR spectrum, the proton peak of the ligand was shifted towards the more downfield region. 15 protons of the methyl group in Cp* appeared at δ 1.751 ppm. In the ^{13}C NMR spectrum, carbon peaks of the ligand were displayed in the range of δ 124.1–150.6 ppm. Methyl carbon and aromatic carbon peaks of Cp* were found to be at δ 8.71 and 89.65 ppm, respectively. The sp^3 C–H stretching fre-

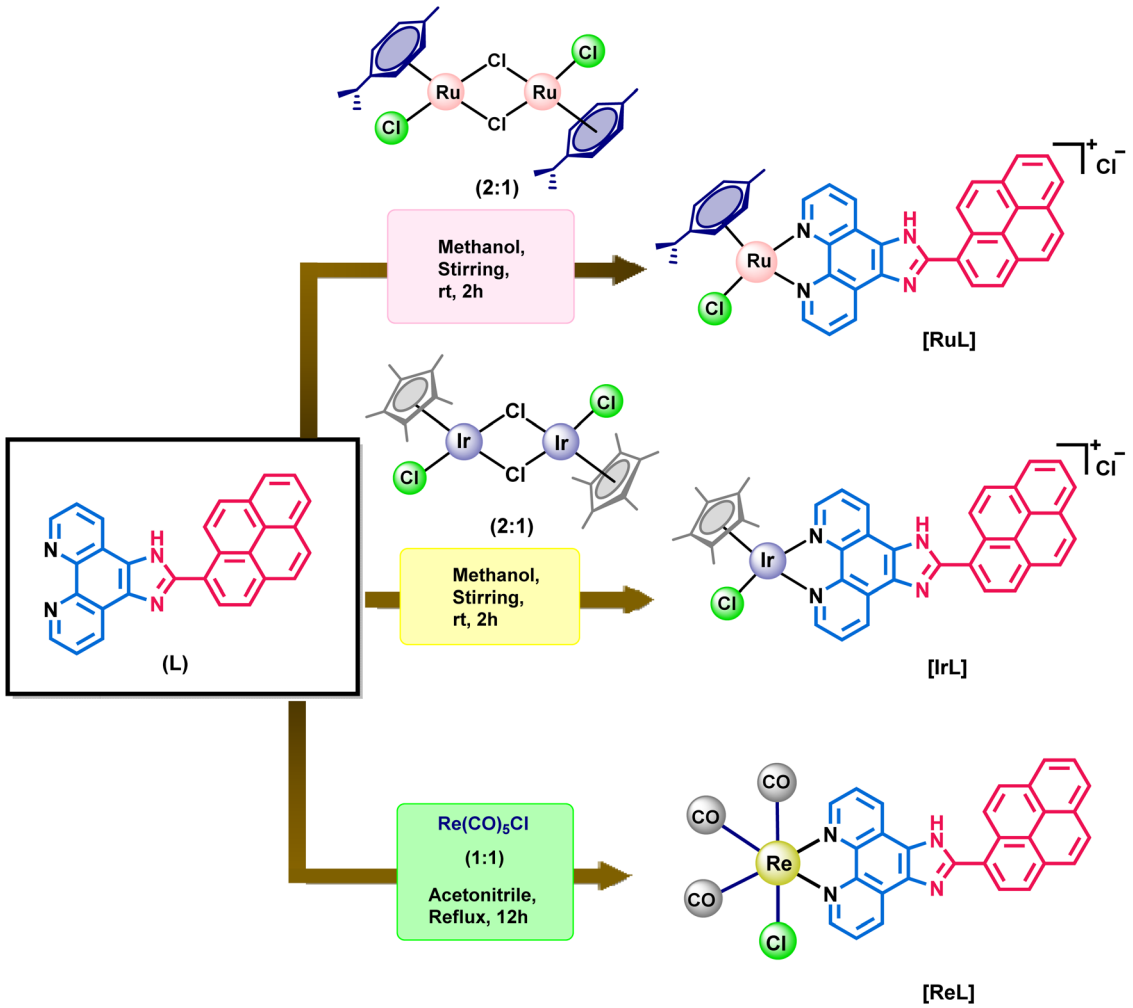

Scheme 2 Synthesis of metal complexes.

quency at 2967 cm^{-1} and sp^3 C–H bending at 1025 cm^{-1} were noted from the IR spectrum, which also supported the existence of the complex. From ESI-MS, the *m*/*z* value 783.1968 $[M–Cl]^+$ exactly matched with the calculated one, and a characteristic isotopic pattern of Ir metal was also observed. A single peak from the complex [**IrL**] in ultra-performance liquid chromatography (UPLC) at a retention time of 2.419 min with a purity of 100% was observed. Ruthenium(II) *p*-cymene [2-(pyrene-1-yl)-1*H*-imidazo[4,5-*f*][1,10]phenanthroline] chloride was synthesized by the treatment of $[(\eta^6\text{-}p\text{-cymene})RuCl(\mu\text{-}Cl)]_2$ (0.5 equiv.) with ligand **L** (1 equiv.) in methanol under stirring for 2 h at room temperature. The structure of this complex was characterized by ^1H and ^{13}C NMR, FT-IR, and HRMS. In the ^1H NMR spectrum, the proton peaks of the ligand were shifted towards the more downfield region. Two peaks of the aromatic proton of *p*-cymene appeared at δ 6.15 ppm and δ 6.39 ppm, the three methyl protons of *p*-cymene moiety were found at δ 0.93 ppm and δ 2.24 ppm, CH protons of the isopropyl groups appeared as multiplet in the region of δ 2.60–2.68 ppm. In the ^{13}C NMR spectrum, ligand peaks were observed at δ 125.4 to δ 154.2 ppm, *p*-cymene carbons ($-CH_3$, –CH) showed at δ 18.8, 22.1, and 30.9 ppm, and *p*-cymene ring carbons were displayed as δ 84.3, 86.8, and 104.3 ppm. The sp^3 C–H stretching frequency at 2962 cm^{-1} and sp^3 C–H bending at 1201 cm^{-1} were noted from the IR spectrum, which also supported the formation of this complex. From ESI-MS, *m*/*z* value 691.1281 $[M - Cl]^+$ exactly matched with the calculated one. One major peak was observed in ultra-performance liquid chromatography (UPLC) at 2.592 min with a purity of 97.34%. Rhenium(I) [2-(pyrene-1-yl)-1*H*-imidazo[4,5-*f*][1,10]phenanthroline] tricarbonyl chloride was synthesized by adding $[Re(CO)_5Cl]$ (1 equiv.) into the acetonitrile solution of ligand L (1 equiv.) followed by stirring in room temperature for 12 h under reflux condition. The formation of this complex was determined by ^1H and ^{13}C NMR, FT-IR, and HRMS. In the ^1H NMR spectrum, ligand protons shifted towards the downfield region. In the ^{13}C NMR spectrum, ligand peaks were observed at δ 123.1 to 151.6 ppm. Carbonyl carbon peaks were found to be at δ 193.9 and 206.6 ppm. In the IR spectrum, the characteristic peak of CO stretching frequency at 2031.09 cm^{-1} and 1915.93 cm^{-1} also confirmed the formation

of this complex. In ESI-MS, the *m*/*z* value 732.1025 $[M - Cl + CH_3CN]^+$ exactly matched the calculated one. Two peaks were observed in ultra-performance liquid chromatography (UPLC) at retention times of 1.994 and 2.847 min with a purity of 81.20% and 18.80%, respectively, with 100% overall purity; and in UV-vis spectrum, the absorbance of both peaks exactly matched, which supported the regioisomer formation (Table 1).

Photophysical properties

Photophysical properties of complex [**RuL**], [**IrL**], and [**ReL**] were studied in 10% DMSO. Here, all three complexes showed an intense π–π* absorption band at 260–325 nm region due to the electronic transition between the lower energy π bonding highest occupied molecular orbital (HOMO) to the higher energy lowest unoccupied π* antibonding molecular orbital (LUMO) of the ligand with a weak absorption band of metal to ligand charge transfer (MLCT) at 330–490 nm region (Fig. S1†).[35] These complexes displayed emission spectra of π–π* excitation in the range of λ_{ems} 360–550 nm and MLCT excitation at λ_{ems} 375–610 nm due to the highly extended conjugation (Fig. S2 and S3†). Here, the quantum yield (φ) 0.187 of [**IrL**] was higher than that of the other two complexes and it was calculated from eqn (i).[36]

Solubility, lipophilicity, and conductivity study

These [**RuL**], [**IrL**] and [**ReL**] complexes are highly soluble in DMSO. Complexes [**RuL**] and [**IrL**] show good solubility in methanol, ethanol, and water and are moderately soluble in acetonitrile but complex [**ReL**] is significantly soluble in acetonitrile and moderately soluble in methanol, ethanol, and water. One of the essential aspects is the balance between lipophilicity and hydrophilicity to establish metal complexes as tumor-shrinking agents. Using the shake flask method, we determined the lipophilic character of all the complexes from the n-octanol/water partition coefficient ($\log P_{o/w}$, where $P_{o/w}$ = the octanol/water partition coefficient).[37] The experimental $\log P_{o/w}$ value of complex [**ReL**] was observed as 0.1669, which is comparatively higher than that for complexes [**RuL**] and [**IrL**].[38] In pure DMSO the molar conductance of complexes [**RuL**], [**IrL**], and [**ReL**] were displayed at 10, 5, and 19 S cm^2 mol^{-1}, respectively.[39] However, the conductance of these complexes increased in 10% DMSO medium (~21–53 S cm^2 mol^{-1}, Table 1). These values signified that in a bulk aqueous medium, the M–Cl bond would be weak, and hence these could bind efficiently with proteins and DNA base pairs.[40]

Stability study

To understand the stability of complexes [**RuL**], [**IrL**] and [**ReL**] in the biological environment, time-dependent UV-visible spectra were recorded with the complexes in GSH (1 mM) and 10% DMSO medium.[41,42] However, we observed a negligible change of absorbance and λ_{max} in both the conditions after 48 hours, which demonstrated that the M–Cl bond of these complexes was extremely stable in a medium with less water content as well as in GSH (Fig. S4 and S5†).[34] ^{1}H NMR and UV Visible spectroscopy was used to investigate the binding ability

Table 1 Photophysical characterization, lipophilicity, and conductivity profiles of complexes [**RuL**], [**IrL**], and [**ReL**]

Sample code	λ^a (nm)		λ^b (nm)		Stock's shift		O.D^c		ε^d (M^{-1} cm^{-1})		φ^e		$\log p_{o/w}{}^f$	Λ^g (Sm^2 M^{-1})	
	π–π*	MLCT	Exiting on π–π*	Exiting on MLCT	Exiting on π–π*	Exiting on MLCT	π–π*	MLCT	π–π*	MLCT	Exiting on π–π*	Exiting on MLCT		DMSO	10% DMSO
RuL	281	361	404, 466	469	123, 105	108	0.879	0.557	29 300	18 583	0.02	0.039	0.0629	10	25
IrL	280	359	401, 467	470	121, 108	111	1.1017	0.536	33 900	17 867	0.187	0.345	0.1072	5	21
ReL	280	377	403, 466	468	123, 89	91	0.693	0.427	23 100	14 233	0.154	0.225	0.1669	19	53
Quinoline sulphate	350		452		102		0.25		8000		0.547				

[a] Absorption maxima. [b] Emission wavelength. [c] Optical density. [d] Extinction coefficient. [e] Quantum yield. [f] *n*-Octanol/water partition coefficient. [g] Conductance in DMSO and 10% aqueous DMSO.

of these complexes with cysteine.[43] In UV Visible spectra, the absorbance of these complexes was also significantly changed with respect to time (Fig. S6†). Herein, ^{1}H NMR of these complexes was recorded in a particular time interval in DMSO-d_6/D_2O mixture and we observed a substantial deviation in the spectra (Fig. S7†).[44,45] Guanine and adenine base pairs interaction with the complexes was also monitored in UV-visible spectroscopy. The spectral change of these complexes with the increasing concentration of the base pairs proved that these complexes effectively bind with DNA base pairs through covalent bonding (Fig. S8†).[46]

DNA binding study

UV-vis spectroscopy. Deoxyribonucleic acid (DNA) is one of the most common targets for anticancer drugs. Covalent and noncovalent (intercalation, groove binding, and electrostatic) interactions are the two distinct ways that metal complexes attach to DNA.[47,48] In this study, the binding affinity of DNA towards complexes was monitored by UV-visible spectroscopy.[49] These complexes exhibited a hypochromic shift in absorbance in π–π* region with increasing DNA concentration from 0–60 μM (Tris-HCl buffer, pH 7.8, t = 25 °C) (Fig. S9†). An isosbestic point appeared after the MLCT region, which supported the covalent interaction of DNA with complexes.[50] The intrinsic binding constant, k_b was calculated from eqn (ii), and complex [**IrL**] exhibited the highest k_b as 0.023 × 10^6 M^{-1}, which is comparatively higher than K_b of [**RuL**], [**ReL**] (Table 2 and Fig. S10†). It can be concluded that complex [**IrL**] strongly intercalates the DNA as k_b of this complex is 1/10th in order of $K_{EtBr\text{-}DNA}$ (7 × 10^5 M^{-1}).[51]

Ethidium bromide binding study

The extent of the intercalation of these complexes was further monitored by ethidium bromide (EtBr) displacement assay using fluorescence spectroscopy (Fig. S11†). In the presence of DNA, EtBr showed fluorescence emission at 600–800 nm region while exciting at 485 nm. In this competitive study, the fluorescence intensity of EtBr was gradually quenched with the increasing DNA concentration, which justified that the complexes intercalated the DNA by replacing EtBr (Fig. S11†). Here, the values of the Stern–Volmer quenching constant (K_{sv}), apparent binding constant (K_{app}), and the number of binding sites (n) were calculated from eqn (iii) and (iv) (Table 2 and Fig. S11†).[51] The K_{SV} values of complex [**RuL**], [**IrL**], and [**ReL**] were found to be 0.0199 × 10^6 M^{-1}, 0.0182 × 10^6 M^{-1}, and 0.0079 × 10^6 M^{-1}, respectively. The values of K_{app} of complex [**RuL**] and [**IrL**] were 2.5 × 10^6 M^{-1} and [**ReL**] 1.42 × 10^6 M^{-1}, respectively.

Viscosity study

An investigation into the viscosity of these complexes with DNA using the hydrodynamic technique unveiled their DNA binding mechanisms.[52] This study was performed to comprehend the change in the relative viscosity of these complexes with a gradual increase in the ratio of complex to ct-DNA using an Ostwald viscometer. A steady increase of viscosity was observed from the plot of $(\eta/\eta_0)^{1/3}$ *vs.* [complex]/[DNA] (Fig. S13†), which clearly signified that complexes efficiently intercalated DNA.[53] Typically, the intercalation facilitated the separation between the DNA base pairs along with the elongation of the DNA strand, which was supported by increased viscosity.

BSA binding study

Bovine serum albumin (BSA) is a serum albumin protein, structurally homologous with human serum albumin (HSA). BSA binding study was accomplished in a spectro-fluorometer to investigate the binding ability of complexes with BSA.[54] Here, fluorescence emission spectra of BSA appeared at 343 nm while exciting at 295 nm. The fluorescence intensity of BSA gradually decreased while increasing the concentration of these complexes (Fig. S14†).[55] K_q and K_{BSA} values were evaluated from the Stern–Volmer equation (eqn (v)). The value of [**IrL**] was 0.0321 × 10^6 M^{-1} relatively higher than 0.029 × 10^6 M^{-1} and 0.02 × 10^6 M^{-1} of [**RuL**] and [**ReL**], whereas the [**RuL**], [**IrL**], and [**ReL**] complexes showed good binding affinity constant (K) of 0.0512 × 10^4 M^{-1}, 0.0231 × 10^4 M^{-1} and 0.0129 × 10^4 M^{-1}, respectively, which were evaluated from the Scatchard plot (eqn (vi)) (Table 3 and Fig. S15†). Significant binding with BSA not only helps for good transportation but also helps the complexes to remain intact in high GSH content.[33]

Singlet oxygen generation ($^1O_2$)

Further investigation into the singlet oxygen production capability of the complexes upon photoactivation by visible light

Table 2 Binding parameters of complexes [**RuL**], [**IrL**], and [**ReL**] for the interaction with ct-DNA

Complex	λ (nm)	Change absorbance intensity	K_b × (10^6 M^{-1})^a	K_{SV} × (10^6 M^{-1})^b	K_{app} × (10^6 M^{-1})^c
[**RuL**]	288	Hypochromism	0.0097	0.0199	2.5
[**IrL**]	300	Hypochromism	0.0232	0.0182	2.5
[**ReL**]	300	Hypochromism	0.0063	0.0079	1.42

^{a} K_b, intrinsic DNA binding constant from UV-vis absorption titration. ^{b} K_{SV}, Stern–Volmer quenching constant. ^{c} K_{app}, apparent DNA binding constant from competitive displacement from fluorescence spectroscopy.

Table 3 Binding parameters of complexes [**RuL**], [**IrL**], and [**ReL**] for the interaction with BSA

Complex	K_{BSA} × (10^6 M^{-1})^a	k_q × (10^{13} M^{-1})^b	K × (10^4 M^{-1})^c	n^d
[**RuL**]	0.029	0.2903	0.05124	1.29
[**IrL**]	0.0321	0.3212	0.02311	1.39
[**ReL**]	0.0208	0.2085	0.0129	1.64

^{a} K_{BSA}, Stern–Volmer quenching constant. ^{b} k_q, quenching rate constant (BSA). ^{c} K, binding constant with BSA. ^{d} n number of binding sites.

Table 4 Light and dark toxicity of all the synthesized complexes

	IC_{50} (μM)[a]					
	MDA-MB-231[b]					
	(In the absence of GSH)			(In the presence of GSH)		
Complex	Dark	In light	PI[c]	Dark	In light	PI
[**RuL**]	25.12 ± 0.69	6.41 ± 0.58	3.92	26.22 ± 0.61	6.89 ± 0.52	3.81
[**IrL**]	23.12 ± 0.73	3.70 ± 0.42	6.25	24.15 ± 1.42	3.90 ± 0.78	6.19
[**ReL**]	28.12 ± 0.12	8.12 ± 1.10	3.46	28.62 ± 0.12	8.82 ± 1.28	3.24
Cisplatin	9.46 ± 0.62	9.23 ± 0.56	1.02	56.6 ± 0.54	57.26 ± 0.48	0.99

[a] IC_{50}: 50% of cells experience cell death. [b] Triple negative human breast cell line. [c] PI: phototoxicity index.

irradiation (400–700 nm) using diphenylisobenzofuran (DPBF) as a singlet oxygen scavenger was carried out and Rose Bengal was used as a reference for the singlet oxygen producer. The respective quantum yields were calculated using eqn (vii) and (viii).[56,57] In UV-visible spectroscopy, the changes in absorbance of DPBF (100 μM) at λ = 415.5 nm in the presence of rose Bengal and complexes (50 μM) under dark and light conditions were recorded. Fig. S16† illustrates the monoexponential decrease in absorbance of DPBF seen at respective λ_{max} during the photosensitizing process carried out in association with RB and other complexes when exposed to visible light. The amount of formation of relative singlet oxygen ($^1O_2$) from complexes was observed from the plot of A/A_0 *vs.* photoexposure time (t) (Fig. S17†).[58] The quantum yield of 0.90 of [**IrL**] was higher than 0.37 and 0.47 of [**RuL**] and [**ReL**], respectively.

***In vitro* cytotoxicity study.** The *in vitro* cytotoxicity tests of all the complexes ([**RuL**], [**IrL**], and [**ReL**]), and control drug cisplatin were performed *via* typical 3-(4,5-dimethylthiazol-2-yl)-2,5-diphenyltetrazolium bromide (MTT) assay protocol using the TNBC cell line (MDA-MB-231) along with an immortalized human embryonic kidney cell line (HEK-293) under dark and light exposure in the presence and absence of GSH in triplicates.[60] The cells were exposed under yellow light (0–2 J cm^{-2}) from a 400 W tungsten lamp fitted with a heat isolation filter and 500 nm long pass filter at an intensity of 4 mW cm^{-2} for 4 hours in the presence of both complexes. However, all the complexes demonstrated insignificant dark toxicity against TNBC cell lines (IC_{50} ~20 μM). These complexes exhibited significant cytotoxic behaviour (IC_{50} ~3–6 μM, PI > 2) in the presence of yellow light compared to dark condition.[58,59] Among the Ru(II), Ir(III), and Re(I) complexes, [**Irl**] exhibited highest potency in TNBC cell line (IC_{50} 3.70 ± 0.42 μM) (Table 2). All these complexes exhibited higher potency and selectivity than cisplatin in both dark and light conditions. Although these complexes exhibited significant potency against cancer cells in normoxia, cytotoxicity may depreciate in the presence of excess GSH environments.[59] Hence, we explored the potency of these complexes in the presence of excess GSH against TNBC cells under dark and light irradiation. However, an insignificant change of potency was observed for all these complexes in the absence and presence of excess GSH (Table 4). The higher potency of these complexes under photo irradiation in normoxia can be ascribed to (i) high log $P_{o/w}$ (ii) high cellular accumulation (iii) low GSH interaction as GSH might be oxidised to GSSG in the presence of $^1O_2$ (iv) strong DNA intercalation and cellular damage by singlet oxygen generation. The insignificant change of cytotoxicity in the presence of excess GSH can be explained in two ways: (i) these complexes displayed high affinity (~10^{13}) to serum albumin, which facilitates the drug delivery and prevents the deactivation from GSH;[34] (ii) slow rate of hydrolysis in excess GSH medium. In contrast, cisplatin displays a huge loss in activity (~70%) under the excess GSH conditions (Table 4).[34] Thereby, it is bringing forth a useful drug in cancer therapy in the presence of light presiding over the prevailing anticancer drug, cisplatin. Interestingly, IC_{50} values for HEK-29 cells are much higher compare to MDA-MB-231 cells, which interprets that complexes selectively, damaged the cancer cells as well (Table S1†).

3. Conclusion

The treatment of TNBC is a challenge for both clinicians and patients due to its worst prognosis in association with fewer treatment strategies having a lack of specific biomarkers for targeted therapies, which enchanted our attention to meticulously synthesize the 2-(pyren-1-yl)-1*H*-imidazo[4,5-*f*][1,10] phenanthroline based phototoxic Ru(II), Ir(III) and Re(I) organometallic complexes, [**RuL**], [**IrL**], [**ReL**] to screen anticancer potential against MDA-MB-231 TNBC cells. The precise analysis enlightened that all three complexes were highly efficient to exhibit cytotoxicity under irradiation of visible light acquiring the ability to interact with DNA bases either through a covalent manner or through intercalation along with the generation of singlet oxygen ($^1O_2$) as ROS. All the complexes showed resistivity towards GSH and in 10% aqueous DMSO medium. Complex [**ReL**] showed the highest lipophilicity (0.1669) compared to the other two complexes, which might be due to the presence of three CO ligands. Moreover, all the complexes were very avid to bind with serum albumin, proving their ability to be transported through the bloodstream.

Among the three complexes, complex [**IrL**] was identified as the best phototoxic scaffold against MDA-MB-231 in the absence and presence of GSH associated with the highest quantum yield (0.90) for $^1O_2$ generation. Also, the complex [**IrL**] displayed a strong binding affinity with DNA and with serum albumin (BSA) displaying the highest binding constant values. Although all the complexes had luminescent properties, complex [**IrL**] was the best among them with the highest quantum yield of fluorescence (0.187). Therefore, it can be predicted that complex [**IrL**] may be successfully utilized for tracking the TNBC cells in the body as well as for selective treatment of TNBC upon irradiation of visible light in the near future.

4. Experimental section

Materials and methods

In all experiments, the reagents and solvents used were of the highest levels of purity and best market grades. All organic solvents used in chromatography and chemical synthesis were of analytical grade, obtained from E. Merck. (India). The required chemicals such as 1,10-phenanthroline-5,6-dione, 1-pyrenecarboxaldehyde, ammonium acetate, ruthenium(II)-(dichloro)-*p*-cymene dimer, iridium(III)-(dichloro)-pentamethyl cyclopentadienyl dimer, and pentacarbonylchloro rhenium were obtained from E-Merck, Sigma Aldrich and Spectrochem. Thin-layer chromatography was accomplished on pre-coated silica gel 60 F254 aluminum sheets (E. Merck, Germany). Bovine serum albumin (BSA) was provided by Sigma Aldrich Chemical Limited. The triple-negative breast cancer (TNBC) cell line, MDA-MB-231, and normal kidney cell lines, HEK-293 used in this work were supplied by the National Center for Cell Science (NCCS), Pune. A 400 MHz Advanced Bruker DPX spectrometer was used to record the ^{1}H and ^{13}C NMR spectra, with tetramethylsilane (TMS) acting as the internal reference. The molecular alterations were measured in ppm units. The abbreviated terms 's' stands for singlet, 'bs' stands for broad singlet, 'd' stands for doublet, 't' stands for triplet, and 'm' stands for multiplet. The melting points of the compounds were measured using an open capillary tube and DT apparatus powered by an Elchem Microprocessor. Viscosity was performed with the help of the Ostwald viscometer and the TDS Conductometer 307 was used to determine the conductivity of the complexes. IR spectra (4000–400 cm^{-1}) were recorded using the Shimadzu Affinity FT-IR spectrometer. The mass spectra of the obtained compounds were recorded on a Shimadzu ESI-MS-4000 mass spectroscopy apparatus using a 4000 triple quadrupole MS and methanol as the solvent. UV-Visible spectra were recorded using a JASCO V-730 and JASCO V-670 spectrophotometer utilizing a 1 cm quartz cell. A 96-well plate and an Elisa reader were used for the cytotoxicity (MTT) test and fluorescence spectra were recorded using a Hitachi F7000 69 and JASCO 8500 fluorescence spectrophotometer fitted with a xenon lamp. Analytical ultra-performance liquid chromatography (UPLC) was performed on an AcquityH uplc class containing a quaternary solvent manager coupled with a sample manager and PDA eλ detector with a C18 column (2.5 μm, 4.6 × 150 mm) with 0.5 mL min^{-1} flow rate.

Synthetic procedure

Synthesis of 2-(pyren-1-yl)-1*H*-imidazo[4,5-*f*][1,10]phenanthroline compounds. Firstly, 50 mg of 1, 10-phenanthroline-5,6-dione (0.238 mmol, 1 equiv.) was dissolved in a minimum volume of glacial acetic acid in a 50 ml pear-shaped round-bottom flask. Next, equimolar amounts (1 : 1) of 1-pyrene carboxaldehyde (1 equiv.) and 8 molar equivalents (excess) of ammonium acetate (146. The reaction mixture was continuously stirred at 120 °C while being held in a reflux state for 30 hours. TLC in pure methanol was used to monitor the reaction and assess product generation. After the reaction was completed, the mixture was placed into a beaker filled with ice-cold water. Ammonia solution was then added dropwise while the mixture was constantly stirred to neutralize the solution and cause precipitation. The precipitate was filtered and dried overnight after being allowed to settle for 12 hours in a refrigerator. It was then repeatedly washed in hexane to remove impurities. Then, with a 90%–94% yield, pure crystalline products in a range of yellow and brown tones were produced. The confirmation of the structures was performed using ^{1}H NMR spectroscopy, IR spectroscopy, and HRMS. Purity was analyzed by HRMS.

2-(Pyren-1-yl)-1*H*-imidazo[4,5-*f*][1,10]phenanthroline. Arylide yellowish solid, Yield: 90% Mp: 216 °C, R_f: 0.66 (1 : 3 ethyl acetate : hexane), ^{1}H NMR (400 MHz, DMSO-d_6): δ = 9.575 (d, J = 9.2 Hz, 1H), 9.096 (m, 4H), 8.713 (d, J = 8 Hz, 1H), 8.551 (d, J = 8 Hz, 1H), 8.415 (m, 3H), 8.325 (d, J = 1.2 Hz, 2H), 8.187 (t, 1H), 1.751 (m, 2H), ^{13}C NMR (101 MHz, DMSO-d_6): δ = 148.42, 144.12, 132.05, 131.40, 131.23, 130.82, 130.35, 129.08, 127.92, 127.82, 127.20, 126.43, 126.09, 125.38, 124.20, 123.90. Ir (cm^{-1}): 3369 (N–H stretching), 3064 (C–H Ar stretching), 2967 (sp^3 C–H stretching), 1607 (C=N stretching), 1451 (C=C stretching), 1402 (C–N stretching), 1025 (C–H aliphatic bending), 734 (C–H Ar bending). MS (HRMS)$_{observed}$: m/z 421.1454 [M]$^+$, 443.1277 [M + Na]$^+$, MS (HRMS)$_{calculated}$: m/z 443.1273 [M + Na]$^+$ and MS (HRMS)$_{observed}$: m/z 443.1277 [M + Na]$^+$.

(2-(Pyren-1-yl)-1*H*-imidazo[4,5-*f*][1,10]phenanthroline)penta methylcyclopentadienyl iridium chloride. 1 equiv. of 2-(pyren-1-yl)-1*H*-imidazo[4,5-*f*][1,10]phenanthroline and 0.5 equiv. of [(η^5-Cp*)IrCl(μ-Cl)]$_2$ were dissolved in methanol in a round bottom flask for 2 h at room temperature. The reaction progress was monitored using TLC and 100% methanol as a solvent system. The reaction mixture turned yellow. After evaporation of the solvent, for purification, the product was washed with hexane and recrystallized in ethanol with a high yield (90–92%). The structure was confirmed by NMR spectroscopy, IR, and HRMS. Purity was analyzed by UPLC and HRMS.

(2-(Pyren-1-yl)-1*H*-imidazo[4,5-*f*][1,10]phenanthroline) penta methylcyclopentadienyl iridium chloride. Yellowish solid, Yield: 91%, Mp: 270 °C, R_f: 0.46 (1 : 3 ethyl acetate : hexane), ^{1}H NMR (400 MHz, DMSO-d_6): δ = 9.512 (m, 3H), 9.367 (d, J = 4.8 Hz,

2H), 8.787 (d, J = 8 Hz, 1H), 8.556 (d, J = 8 Hz, 1H), 8.424 (m, 3H), 8.329 (m, 4H), 8.193 (t, 1H), 1.751 (s, 15H). ^{13}C NMR (101 MHz, DMSO-d_6): δ = 150.57, 144.58, 133.59, 131.33, 130.72, 129.41, 129.20, 128.16, 128.00, 127.79, 127.32, 126.33, 125.62, 125.45, 124.76, 124.07, 89.65, Ir (cm^{-1}): 3369 (N–H stretching) 3064 (C–H Ar stretching), 2967(sp^3 C–H stretching), 1607 (C═N stretching), 1452 (C═C stretching), 1407 (C–N stretching), 1025 (C–H aliphatic bending), 699 (C–H Ar bending), MS $(HRMS)_{calculated}$: m/z 783.1866 $[M - Cl]^+$ and MS $(HRMS)_{observed}$: m/z 783.1968

(2-(Pyren-1-yl)-1*H*-imidazo[4,5-*f*][1,10]phenanthroline) *p*-cymene ruthenium chloride. Similarly, 1 equiv. of 2-(pyren-1-yl)-1*H*-imidazo[4,5-*f*][1,10]phenanthroline and 0.5 equiv. of $[(\eta^6$-*p*-cymene)$RuCl(\mu\text{-}Cl)]_2$ were dissolved in methanol in a round bottom flask for 2 h at room temperature and the progress was monitored using TLC with 100% methanol as a solvent system. The reaction mixture turned brownish-yellow. For purification, the product was washed with hexane and recrystallized in ethanol with a high yield (90–92%). The structure was confirmed with the help of NMR spectroscopy, IR, and HRMS. Purity was analyzed by UPLC and HRMS.

(2-(Pyren-1-yl)-1*H*-imidazo[4,5-*f*][1,10]phenanthroline) *p*-cymene ruthenium chloride. Brown yellowish solid, Yield: 90% Mp: 229 °C, R_f: 0.49 (1 : 3 ethyl acetate : hexane), ^{1}H NMR (400 MHz, DMSO-d_6): δ = 9.906 (d, J = 5.2 Hz, 2H), 9.543(d, J = 9.2 Hz, 1H), 9.441(d, J = 7.6 Hz, 2H), 8.792(d, J = 8 Hz, 1H), 8.524 (d, J = 8 Hz, 1H), 8.405 (m, 3H), 8.308 (d, J = 4 Hz, 2H), 8.276 (m, 2H), 8.176 (m, 1H), 6.387 (d, J = 6.4 Hz, 2H), 6.147 (d, J = 6.4 Hz, 2H), 2.675 (m, 1H), 2.237 (s, 3H), 0.929 (d, J = 6.8 Hz, 6H). ^{13}C NMR (101 MHz, DMSO-d_6): δ = 154.23, 143.67, 133.17, 131.36, 123.26, 128.24, 127.80, 127.24, 126.71, 126.21, 125.40, 104.28, 86.79, 84.36, 30.90, 22.14, 18.81. Ir (cm^{-1}): 3362 (N–H stretching) 3045 (C–H Ar stretching), 2962 (sp^3 C–H stretching), 1600 (C═N stretching), 1459 (C═C stretching), 1365 (C–N stretching), 1201 1086 1056 (C–H aliphatic bending), 709 (C–H Ar bending). MS $(HRMS)_{calculated}$: m/z 691.1202 $[M - Cl]^+$, MS $(HRMS)_{observed}$: m/z 691.1281 $[M - Cl]^+$.

(2-(Pyren-1-yl)-1*H*-imidazo[4,5-*f*][1,10]phenanthroline) pentacarbonyl rhenium chloride. 1 equiv. of rhenium(I) pentacarbonyl chloride was dissolved in acetonitrile in a round bottom flask and 1 equiv. of 2-(pyren-1-yl)-1*H*-imidazo[4,5-*f*][1,10]phenanthroline was added and refluxed for 12 h at 80 °C. The reaction progress was monitored using TLC. The reaction mixture turned yellow. Work-up was performed by evaporating the solvent and hexane wash was given to remove the impurities. Recrystallization was performed in methanol/diethyl ether for further purification with 89–90% yield. The compound structure was confirmed by NMR spectroscopy, IR, and HRMS. Purity was analyzed by UPLC and HRMS.

(2-(Pyren-1-yl)-1*H*-imidazo[4,5-*f*][1,10]phenanthroline) pentacarbonyl rhenium chloride. Yellowish solid, Yield: 90% Mp: 301 °C, R_f: 0.53 (1 : 3 ethyl acetate : hexane), ^{1}H NMR (400 MHz, DMSO-d_6): δ = 9.481 (d, J = 9.2 Hz, 1H), 9.424 (d, J = 9.2 Hz, 4H), 8.692 (d, J = 8 Hz, 1H), 8.556 (d, J = 8 Hz, 1H), 8.414 (m, 3H), 8.343 (m, 2H), 8.223 (m, 3H). ^{13}C NMR (101 MHz, DMSO-d_6): δ = 206.61, 193.89, 151.62, 133.39, 132.05, 131.51, 131.28, 131.08, 131.03, 130.06, 129.23, 128.94, 127.84, 127.62, 127.23, 126.83, 126.47, 126.14, 125.67, 125.24, 124.81, 123.05. Ir (cm^{-1}): 3360 (N–H stretching), 3091 (C–H Ar stretching), 2927 (sp^3 C–H stretching), 2031 1915 (C≡O stretching), 1600 (C═N stretching), 1459 (C═C stretching), 1365 (C–N stretching), 1201 1086 1056 (C–H aliphatic bending), 709 (C–H Ar bending). MS $(HRMS)_{calculated}$: m/z 732.1045 $[M - Cl + CH_3CN]^+$, MS $(HRMS)_{observed}$: m/z 732.1025 $[M - Cl + CH_3CN]^+$.

Conflicts of interest

There are no conflicts to declare.

Acknowledgements

The authors are grateful to VIT for 'VIT SEED GRANT'. We acknowledge DST, New Delhi, India for the DST-FIST project. The authors are grateful to the Department of Science and Technology, Government of India for supporting the work through the DST-SERB CRG project grant (CRG/2021/002267).

References

1 M. A. Medina, G. Oza, A. Sharma, L. G. Arriaga, J. M. H. Hernández, V. M. Rotello and J. T. Ramirez, Triple-negative breast cancer: A review of conventional and advanced therapeutic strategies, *Int. J. Environ. Res. Public Health*, 2020, **17**, 2078.

2 L. E. McLemore, C. T. Albarracin, S. K. Gruschkus, R. L. Bassett Jr., Y. Wu, S. Dhamne, I. Yim, K. Lin, I. Bedrosian, N. Sneige and H Chen, HER2 testing in breast cancers: Comparison of assays and interpretation using ASCO/CAP 2013 and 2018 guidelines, *Breast Cancer Res. Treat.*, 2021, **187**, 95–104.

3 S. Shiovitz and L. A. Korde, Genetics of breast cancer: A topic in evolution, *Ann. Oncol.*, 2015, **26**, 1291–1299.

4 (*a*) A. Shahbandi, H. D. Nguyen and J. G. Jackson, TP53 mutations and outcomes in breast cancer: Reading beyond the headlines, *Trends Cancer*, 2020, **6**, 98–110; (*b*) G. Corso, P. Veronesi, V. Sacchini and V. Galimberti, Prognosis and Outcome in CDH1-Mutant Lobular Breast Cancer, *Eur. J. Cancer Prev.*, 2018, **27**, 237–238.

5 T. J. Key, P. N. Appleby, G. K. Reeves, R. C. Travis, A. J. Alberg, A. Barricarte, F. Berrino, V. Krogh, S. Sieri, L. A. Brinton, J. F. Dorgan, L. Dossus, M. Dowsett, A. H. Eliassen, R. T. Fortner, S. E. Hankinson, K. J. Helzlsouer, J. Hoffman-Bolton, R. Kaaks, L. L. Kahle, K. Koenig, A. Zeleniuch-Jacquotte, P. Muti, K. Overvad, P. H. M. Peeters, E. Riboli, S. Rinaldi, D. E. Rollison, H. L. Moffitt, D. Trichopoulos, S. S. Tworoger and P. Vineis, Sex hormones and risk of breast cancer in premenopausal women: A collaborative reanalysis of individual participant data from seven prospective studies, *Lancet Oncol.*, 2013, **14**, 1009–1019.

6 C. K. Anders and L. A. Carey, Biology, metastatic patterns and treatment of patients with triple-negative breast cancer, *Clin. Breast Cancer*, 2009, **9**, 73–81.
7 X. Zhang, S. S. Tworoger, A. H. Eliassen and S. E. Hankinson, Postmenopausal Plasma Sex hormone levels and breast cancer risk over 20 years of follow-up, *Breast Cancer Res. Treat.*, 2013, **137**, 883–892.
8 K. Liu, W. Zhang, Z. Dai, M. Wang, T. Tian, X. Liu, H. Kang, H. Guan, S. Zhang and Z. Dai, Association between body mass index and breast cancer risk: Evidence based on a dose–response meta-analysis, *Cancer Manage. Res.*, 2018, **10**, 143–151.
9 X. Wang, T.-L. Hui, M.-Q. Wang, H. Liu, R.-Y. Li and Z.-C. Song, Body Mass index at Diagnosis as a prognostic factor for early-stage invasive breast cancer after surgical resection, *Oncol. Res. Treat.*, 2019, **42**, 190–196.
10 L. Zhang, H. Xu, X. Wu, W. Huang, T. Zhang, P. Hao, B. Peng and X. Zan, A strategy to fight against triple-negative breast cancer: pH-responsive hexahistidine-metal assemblies with high-payload drugs, *ACS Appl. Bio Mater.*, 2020, **3**, 5331–5341.
11 (*a*) N. Berrada, S. Delaloge and F. André, Treatment of triple-negative metastatic breast cancer: Toward individualized targeted treatments or chemosensitization?, *Ann. Oncol.*, 2010, **21**, 30–35; (*b*) F. O. Ademuyiwa, M. J. Ellis and C. X. Ma, Neoadjuvant therapy in operable breast cancer: application to triple negative breast cancer, *J. Oncol.*, 2013, **2013**, 1–6.
12 G. Shumi, T. Desalegn, T. B. Demissie, V. P. Ramachandran and R. Eswaramoorthy, Metal complexes in target-specific anticancer therapy: Recent trends and challenges, *J. Chem.*, 2022, **2022**, 1–19.
13 U. Ndagi, N. Mhlongo and M. E. Soliman, Metal complexes in cancer therapy – an update from drug design perspective, *Drug Des., Dev. Ther.*, 2017, **11**, 599–616.
14 S. Pete, N. Roy, B. Kar and P. Paira, Construction of homo and heteronuclear Ru(II), Ir(III) and Re(I) complexes for target specific cancer therapy, *Coord. Chem. Rev.*, 2022, **460**, 214462.
15 (*a*) N. J. Farrer, L. Salassa and P. J. Sadler, Photoactivated chemotherapy (PACT): the potential of excited-state d-block metals in medicine, *Dalton Trans.*, 2009, **48**, 10690–10701; (*b*) V. Ramu, A. B. Auyeung and S. Bonnet, Cytotoxicity of metal-based photoactivated chemotherapy (PACT) compounds, *Photodyn. Ther.*, 2022, **2451**, 245–258; (*c*) S. Bonnet, Why develop photoactivated chemotherapy?, *Dalton Trans.*, 2018, **47**, 10330–10343.
16 S. Monro, K. L. Colón, H. Yin, J. Roque, P. Konda, S. Gujar, R. P. Thummel, L. Lilge, C. G. Gameron and S. A. McFarland, Transition metal complexes and photodynamic therapy from a tumor-centered approach: Challenges, opportunities, and highlights from the development of TLD1433, *Chem. Rev.*, 2019, **119**, 797–828.
17 (*a*) Q. Sun, Y. Li, H. Shi, Y. Wang, J. Zhang and Q. Zhang, Ruthenium complexes as promising candidates against lung cancer, *Molecules*, 2021, **26**, 4389; (*b*) S. Y. Lee, C. Y. Kim and T.-G. Nam, Ruthenium complexes as anticancer agents: A brief history and perspectives, *Drug Des., Dev. Ther.*, 2020, **14**, 5375–5392.
18 Y. Chen, L. Bai, P. Zhang, H. Zhao and Q. Zhou, The development of Ru(II)-based photoactivated chemotherapy agents, *Molecules*, 2021, **26**, 5679.
19 A. Busemann, I. Flaspohler, X.-Q. Zhou, C. Schmidt, S. K. Goetzfried, V. H. S. van Rixel, I. Ott, M. A. Siegler and S. Bonnet, Ruthenium-based PACT agents based on bisquinoline chelates: Synthesis, photochemistry, and cytotoxicity, *J. Biol. Inorg. Chem.*, 2021, **26**, 667–674.
20 C. Fayad, H. Audi, R. S. Khnayzer and C. F. Daher, The anticancer effect of series of strained photoactivatable Ru(II) polypyridyl complexes on non-small-cell lung cancer and triple negative breast cancer cells, *J. Biol. Inorg. Chem.*, 2021, **26**, 43–55.
21 R. Guan, L. Xie, L. Ji and H. Chao, Phosphorescent iridium (III) complexes for anticancer applications, *Eur. J. Inorg. Chem.*, 2020, **2020**, 3978–3986.
22 Z. Liu, J. Li, X. Ge, S. Zhang, Z. Xu and W. Gao, Design, synthesis, and evaluation of phosphorescent Ir(III) complexes with anticancer activity, *J. Inorg. Biochem.*, 2019, **197**, 110703.
23 P. Zhang, H. Huang, S. Banerjee, G. J. Clarkson, C. Ge, C. Imberti and P. J. Sadler, Nucleus–targeted organoiridium–albumin conjugate for photodynamic cancer therapy, *Angew. Chem., Int. Ed.*, 2019, **58**, 2350–2354.
24 H. Xiang, H. Chen, H. P. Tham, S. Z. F. Phua, J.-G. Liu and Y. Zhao, Cyclometalated iridium(III)-complex-based micelles for glutathione-responsive targeted chemotherapy and photodynamic therapy, *ACS Appl. Mater. Interfaces*, 2017, **9**, 27553–27562.
25 H. S. Liew, C.-W. Mai, M. Zulkefeli, T. Madheswaran, L. V. Kiew, N. Delsuc and M. L. Low, Recent emergence of rhenium(I) tricarbonyl complexes as photosensitisers for cancer therapy, *Molecules*, 2020, **25**, 4176.
26 S. Hostachy, C. Policar and N. Delsuc, Re(I) carbonyl complexes: Multimodal platforms for inorganic chemical biology, *Coord. Chem.*, 2017, **351**, 172–178.
27 A. Leonidova, V. Pierroz, R. Rubbiani, J. Heier, S. Ferrari and G. Gasser, Towards cancer cell-specific phototoxic organometallic rhenium(I) complexes, *Dalton Trans.*, 2014, **20**, 4287–4289.
28 A. Kastl, S. Dieckmann, K. Wähler, T. Völker, L. Kastl, A. L. Merkel, A. Vultur, B. Shannan, K. Harms, M. Ocker, W. J. Parak, M. Herlyn and E. Meggers, Rhenium complexes with visible-light-induced anticancer activity, *ChemMedChem*, 2013, **8**, 924–927.
29 S. C. Marker, S. N. MacMillan, W. R. Zipfel, Z. Li, P. C. Ford and J. J. Wilson, Photoactivated in vitro anticancer activity of rhenium(I) tricarbonyl complexes bearing water-soluble phosphines, *Inorg. Chem.*, 2018, **57**, 1311–1331.
30 D. Bandyopadhyay, J. C. Granados, J. D. Short and B. K. Banik, Polycyclic aromatic compounds as anticancer agents: Evaluation of synthesis and *in vitro* cytotoxicity, *Oncol. Lett.*, 2012, **3**, 45–49.

31 B. K. Banik and F. F. Becker, Polycyclic aromatic compounds as anticancer agents: Structure-activity relationships of chrysene and pyrene derivatives, *Bioorg. Med. Chem.*, 2001, **9**, 593–605.
32 R. Bonsignore, A. Notaro, A. M. P. Salvo, A. Spinello, G. Fiasconaro, A. Terenzi, F. Giacalone, B. K. Keppler, M. Giuliano, M. Gruttadauria and G. Barone, DNA-binding and anticancer activity of pyrene-imidazolium derivatives, *ChemistrySelect*, 2016, **1**, 6755–6761.
33 A. Mondal and P. Paira, Hypoxia efficient and glutathione-resistant cytoselective ruthenium(II)-*p*-cymene-arylimidazo-phenanthroline complexes: Biomolecular interaction and live cell imaging, *Dalton Trans.*, 2020, **49**, 12865–12878.
34 B. Kar, U. Das, S. De, S. Pete, A. S. Sharma, N. Roy, S. K. Ashok Kumar, D. Panda and P. Paira, GSH-resistant and highly cytoselective ruthenium(II)-*p*-cymene-(imidazo [4,5-f][1,10]phenanthrolin-2-yl)phenol complexes as potential anticancer agents, *Dalton Trans.*, 2021, **50**, 10369–10373.
35 (*a*) C. Jin, J. Liu, Y. Chen, L. Zeng, R. Guan, C. Ouyang, L. Ji and H. Chao, Cyclometalated iridium(III) complexes as two-photon phosphorescent probes for specific mitochondrial dynamics tracking in living cells, *Chem. – Eur. J.*, 2015, **21**, 12000–12010; (*b*) Y. Chen, L. Qiao, L. Ji and H. Chao, Phosphorescent iridium(III) complexes as multicolor probes for specific mitochondrial imaging and tracking, *Biomaterials*, 2014, **35**, 2–13.
36 Y. Feng, T. Bai, H. Yan, F. Ding, L. Bai and W. Feng, High fluorescence quantum yield based on the through-Space conjugation of hyperbranched polysiloxane, *Macromolecules*, 2019, **52**, 3075–3082.
37 A. Gilewska, B. Barszcz, J. Masternak, K. Kazimierczuk, J. Sitkowski, J. Wietrzyk and E. Turlej, Similarities and differences in d^6 low-spin ruthenium, rhodium and iridium half-sandwich complexes: Synthesis, structure, cytotoxicity and interaction with biological targets, *J. Biol. Inorg. Chem.*, 2019, **24**, 591–606.
38 M. Kubanik, H. Holtkamp, T. Söhnel, S. M. F. Jamieson and C. G. Hartinger, Impact of the halogen substitution pattern on the biological activity of organoruthenium 8-hydroxyquinoline anticancer agents, *Organometallics*, 2015, **34**, 5658–5668.
39 I. Ali, W. A. Wani and K. Saleem, Empirical formulae to molecular structures of metal complexes by molar conductance, *Synth. React. Inorg., Met.-Org., Nano-Met. Chem.*, 2013, **43**, 1162–1170.
40 W. J. Geary, The use of conductivity measurements in organic solvents for the characterisation of coordination compounds, *Coord. Chem. Rev.*, 1971, **7**, 81–122.
41 I. Romero-Canelón and P. J. Sadler, Next-generation metal anticancer complexes: Multitargeting via redox modulation, *Inorg. Chem.*, 2013, **52**, 12276–12291.
42 N. Roy, U. Sen, Y. Madaan, V. Muthukumar, S. Varddhan, S. K. Sahoo, D. Panda, B. Bose and P. Paira, Mitochondria-targeting click-derived pyridinyltriazolylmethylquinoxaline-based Y-shaped binuclear luminescent ruthenium(II) and iridium(III) complexes as cancer theranostic agents, *Inorg. Chem.*, 2020, **59**, 17689–17711.
43 A. Rigo, A. Corazza, M. Luisa Di Paolo, M. Rossetto, R. Ugolini and M. Scarpa, Interaction of copper with cysteine: Stability of cuprous complexes and catalytic role of cupric ions in anaerobic thiol oxidation, *J. Inorg. Biochem.*, 2004, **98**, 1495–1501.
44 S. Moon, M. Hanif, M. Kubanik, H. Holtkamp, T. Söhnel, S. M. F. Jamieson and C. G. Hartinger, Organoruthenium and osmium anticancer complexes bearing a maleimide functional group: Reactivity to cysteine, stability, and cytotoxicity, *ChemPlusChem*, 2015, **80**, 231–236.
45 S. Enriquez, M. Yu, B. S. Bouley, D. Xie and E. L. Que, Copper(II) complexes for cysteine detection using ^{19}F magnetic resonance, *Dalton Trans.*, 2018, **47**, 15024–15030.
46 L. T. Babu and P. Paira, 9-arylacenaphtho [1,2-b] quinoxalines via Suzuki coupling reaction as cancer therapeutic and cellular imaging agents, *New J. Chem.*, 2021, **45**, 20447–20458.
47 D. Herebian and W. S. Sheldrick, Synthesis and DNA binding properties of bioorganometallic (η^5-pentamethylcyclopentadienyl) iridium(III) complexes of the type $[(\eta^5\text{-}C_5Me_5)Ir(Aa)(dppz)]^{n+}$ (dppz = dipyrido[3,2-a:2′,3′-c]phenazine, n = 1–3), with S-coordinated amino acids (Aa) or peptides, *J. Chem. Soc., Dalton Trans.*, 2002, 966–974.
48 Z.-C. Liu, B.-D. Wang, Z.-Y. Yang, Y. Li, D.-D. Qin and T.-R. Li, Synthesis, crystal structure, DNA interaction and antioxidant activities of two novel water-soluble Cu(2+) complexes derivated from 2-oxo-quinoline-3-carbaldehyde schiff-bases, *Eur. J. Med. Chem.*, 2009, **44**, 4477–4484.
49 P. Selvam, S. De, P. Paira, S. K. Ashok Kumar, S. Kumar R, A. Moorthy, A. Ghosh, Y.-C. Kuo, S. Banerjee and S. K. Jenifer, In vitro studies on the selective cytotoxic effect of luminescent Ru(II)-*p*-cymene complexes of imidazo-pyridine and imidazo quinoline ligands, *Dalton Trans.*, 2022, **51**, 17263–17276.
50 M. Sirajuddin, S. Ali and A. Badshah, Drug-DNA interactions and their study by UV-Visible, fluorescence spectroscopies and cyclic voltammetry, *J. Photochem. Photobiol., B*, 2013, **124**, 1–19.
51 N. Roy, U. Sen, S. R. Chaudhuri, V. Muthukumar, P. Moharana, P. Paira, B. Bose, A. Gauthaman and A. Moorthy, Mitochondria specific highly cytoselective iridium(III)–Cp* dipyridophenazine (dppz) complexes as cancer cell imaging agents, *Dalton Trans.*, 2021, **50**, 2268–2283.
52 N. Shahabadi and S. Mohammadi, Binding studies of a new water-soluble iron(III) schiff base complex to DNA using multispectroscopic methods, *Bioinorg. Chem. Appl.*, 2012, **2012**, 1–9, DOI: **10.1155/2012/571913**.
53 Z. C. Liu, B. D. Wang, Z. Y. Yang, Y. Li, D. D. Qin and T. R. Li, Synthesis, crystal structure, DNA interaction and antioxidant activities of two novel water-soluble Cu(2+) complexes derivated from 2-oxo-quinoline-3-carbaldehyde schiff-bases, *Eur. J. Med. Chem.*, 2009, **44**, 4477–4484.
54 A. Mondal, U. Sen, N. Roy, V. Muthukumar, S. K. Sahoo, B. Bose and P. Paira, DNA targeting half sandwich Ru(II)-*p*-

cymene-N^ N complexes as cancer cell imaging and terminating agents: Influence of regioisomers in cytotoxicity, *Dalton Trans.*, 2021, **50**, 979–997.

55 P. K. Anuja and P. Paira, Luminescent anticancer Ru(II)-arenebipyridine and phenanthroline complexes: Synthesis, characterization, DFT studies, biological interactions and cellular imaging application, *J. Inorg. Biochem.*, 2020, **208**, 111099.

56 A. Bhattacharyya, A. Dixit, S. Banerjee, B. Roy, A. Kumar, A. A. Karande and A. R. Chakravarty, BODIPY appended copper(II) complexes for cellular imaging and singlet oxygen mediated anticancer activity in visible light, *RSC Adv.*, 2016, **6**, 104474–104482.

57 D. Musib, M. Pal, M. K. Raza and M. Roy, Photo-physical, theoretical and photo-cytotoxic evaluation of a new class of lanthanide(III)–curcumin/diketone complexes for PDT application, *Dalton Trans.*, 2020, **49**, 10786–10798.

58 B. Kar and P. Paira, One pot three component synthesis of DNA targeting phototoxic Ru(II)-*p*-cymene dipyrido[3,2-a:2′,3′-c]phenazine analogues, *Dalton Trans.*, 2022, **51**, 15686–15695.

59 N. J. Farrer, J. A. Woods, L. Salassa, Y. Zhao, K. S. Robinson, G. Clarkson, F. S. Mackay and P. J. Sadler, A potent trans-diimine platinum anticancer complex photoactivated by visible light, *Angew. Chem.*, 2010, **122**, 9089–9092.

60 B. Kar, S. Shanavas, A. H. Nagendra, U. Das, N. Roy, S. Pete, A. Sharma, S. De, S. K. Ashok Kumar, S. Vardhan, S. K. Sahoo, D. Panda, S. Shenoy, B. Bose and P. Paira, Iridium(III)–Cp*-(imidazo [4, 5-f][1, 10] phenanthrolin-2-yl) phenol analogues as hypoxia active, GSH-resistant cancer cytoselective and mitochondria-targeting cancer stem cell therapeutic agents, *Dalton Trans.*, 2022, **51**, 5494–5514.